This preprint is accepted for publication at

Sajjadinia, S.S., Carpentieri, B., Holzapfel, G.A. (2024). Large-Scale Finite Element Modeling of Pre-stress in Articular Cartilage. In: Skalli, W., Laporte, S., Benoit, A. (eds) Computer Methods in Biomechanics and Biomedical Engineering II. CMBBE 2023. Lecture Notes in Computational Vision and Biomechanics, vol 39. Springer, Cham. https://doi.org/10.1007/978-3-031-55315-8_12.

Large-Scale Finite Element Modeling of Pre-Stress in Articular Cartilage

Seyed Shayan Sajjadinia[1,⋆], Bruno Carpentieri[1], and Gerhard A. Holzapfel[2,3]

[1] Faculty of Engineering, Free University of Bozen-Bolzano, Italy,
[2] Institute of Biomechanics, Graz University of Technology, Austria,
[3] Department of Structural Engineering, Norwegian University of Science and Technology, Norway

Abstract. Finite element (FE) methods and multiphasic equations are commonly used to model articular cartilage (AC). This tissue has a fixed negative charge that leads to osmotic pressure in its structure, causing pre-stress. A challenge in FE modeling of AC is to start the simulation with the correct *in vivo* pre-stressed state of the tissue, which is traditionally handled by custom optimizers, the so-called pre-stressing algorithm (PSA). These algorithms, which have been successfully implemented in small-scale models, detect either the geometrical stress-free state, constitutive stress-free state, or both. Therefore, this work aims to extend it to a larger-scale AC model in a human tibiofemoral joint, developed using depth-dependent and multiphasic equations of AC. We employed a unified optimizer, rather than sequential optimizers, to reduce the number of algorithmic iterations. Also, fibrillar orientations and other microstructural properties of the AC substructures are approximated by defining the approximate normalized depth. The pre-stressed state is calculated in around six hours, revealing the noted depth-dependent stresses. To facilitate future research, the PSA is open-sourced at https://github.com/shayansss/psa.

Keywords: pre-stressing optimizer, articular cartilage, large-scale finite element analysis

1 Introduction

The articular cartilage (AC) in the human knee permits lubricated and smooth bone contact. This tissue is composed of a mixture of fibril-reinforced and non-fibrillar components and a charged biphasic medium that can be modeled by finite element (FE) analysis. Due to its electrochemical characteristics and in particular its osmotic pressure, the solid AC matrix withstands a pre-stress even without external load [12].

When modeling the AC pre-stressing using regular FE methods, the initial state of the model changes as the tissue expands to equilibrium (when the AC

⋆ Corresponding author at: Faculty of Engineering, Free University of Bozen-Bolzano, 39100 Bozen-Bolzano, Italy; e-mail: ssajjadinia@unibz.it

fibrils are stretched). Since this initial *in vivo* (stress-free) state is unknown, inverse FE methods (or more precisely, fixed-point-based backward optimizers) are commonly used to approximate this state [14, 9]. These algorithms are very simple compared to the other methods but still very iterative.

In particular, it has been shown that with two different optimizers (one for calculating the initial geometry and the other for calculating the initial material parameters), the stress-free state could be approximated in small-scale AC models [9]. Therefore, the present work aims to extend this approach to a larger-scale cartilage model, specifically to the AC substructures of a tibiofemoral joint. We used a pre-stressing algorithm (PSA) with a unified optimizer. Additionally, this work attempts to simulate the pre-stressed state at this larger scale to elucidate its significance for biomechanical simulation.

2 Materials and Methods

In this section, the superscript REF refers to the known (experimentally observed) values once the FE model is pre-stressed and reaches equilibrium, while subscript 0 refers to the initial state of an FE analysis. Furthermore, the superscript (t) refers to the values at step t of the pre-stressing iterative algorithm that attempts to approximate the stress-free state of the affected parameters.

2.1 Constitutive modeling

The total stress tensor $\boldsymbol{\sigma}$ is calculated using the biphasic theory as follows [7]

$$\boldsymbol{\sigma} = \boldsymbol{\sigma}^{\mathrm{EFF}} - p\mathbf{I}. \tag{1}$$

Here, p is the fluid pressure, $\mathbf{I}$ is the unit identity tensor, and $\boldsymbol{\sigma}^{\mathrm{EFF}}$ is the (effective) solid stress. Given the superscripts MAT, COL, and GAG, representing the contribution of the non-fibrillar matrix, fibrillar network, and osmotic pressure, respectively, we then use the constrained mixture theory [13, 8], i.e.,

$$\boldsymbol{\sigma}^{\mathrm{EFF}} = \boldsymbol{\sigma}^{\mathrm{COL}} + \boldsymbol{\sigma}^{\mathrm{MAT}} - \boldsymbol{\sigma}^{\mathrm{GAG}}, \tag{2}$$

where [9]

$$\boldsymbol{\sigma}^{\mathrm{COL}} = \frac{\emptyset_0^S}{J} \sum_{I=1}^{9} \left[\lambda^I \rho_C^I \left(E_0 + E_\varepsilon \varepsilon^I \right) \varepsilon^I \mathbf{n}^I \otimes \mathbf{n}^I \right] \qquad \text{if } \varepsilon^{\mathrm{I}} > 0, \tag{3}$$

$$\begin{aligned} \boldsymbol{\sigma}^{\mathrm{MAT}} = \emptyset_0^S \frac{G_m \left(1 - \rho_0^{\mathrm{COL}}\right)}{J} \Bigg[-\frac{\ln J}{6} \left(3\emptyset_0^S \frac{J \ln J}{\left(J - \emptyset_0^S\right)^2} - 1 - 3\frac{J + \emptyset_0^S}{J - \emptyset_0^S} \right) \mathbf{I} \\ + \left(\mathbf{F}\mathbf{F}^{\mathrm{T}} - J^{2/3}\mathbf{I} \right) \Bigg], \end{aligned} \tag{4}$$

$$\boldsymbol{\sigma}^{\mathrm{GAG}} = \alpha_1 \left(\frac{1}{J} \right)^{\alpha_2} \mathbf{I}. \tag{5}$$

Here, we have assumed that the AC has 9 predominant fibrillar bundles, including 7 secondary and 2 primary fibrils [16]. For the I-th bundle, the unit direction, logarithmic strain, volume fraction, and elongation are represented as $\mathbf{n}^I$, ε^I, ρ_C^I, and λ^I, respectively. The deformation gradient $\mathbf{F}$ is the partial derivative of the deformed coordinates $\mathbf{x}$ relative to the undeformed coordinates, which also gives the volume ratio $J = \det\mathbf{F}$. The values of the total collagen and solid volume fractions are denoted by ρ^{COL} and $\emptyset^{\mathrm{S}}$, respectively, while the other parameters are material constants. Then the pre-stress before equilibrium $\boldsymbol{\sigma}_0$ can be calculated from (5) by assuming no initial deformation ($\mathbf{F}_0 = \mathbf{I}$) and no initial fluid pressure, i.e.

$$\boldsymbol{\sigma}_0 = -\alpha_1 \mathbf{I} > 0. \tag{6}$$

Due to the soft nature of AC, this matrix deforms until an equilibrium is reached where no further changes in the material occur. With this deformation of the AC, the material fractions and the fibrillar orientation must be altered [15, 13], as

$$\mathbf{n} = \frac{\mathbf{F}\mathbf{n}_0}{\|\mathbf{F}\mathbf{n}_0\|_2}, \tag{7}$$

$$\forall \varphi \in \left\{\emptyset^{\mathrm{S}},\ \rho^{\mathrm{COL}}\right\},\ \varphi = \frac{\varphi_0}{J}, \tag{8}$$

where $\|\ \|_2$ denotes the L2 norm [9]. On the other hand, these material properties are depth-dependent [16], such as the anisotropic fibrillar orientations, which are parallel to the AC surface in the superficial zone but perpendicular to the calcified cartilage in the deep zone. These heterogeneous parameters are therefore determined by the normalized depth z (relative to the AC surface).

Accordingly, we modify the definition of the normalized depth so that it can be used in large-scale AC models with highly heterogeneous thicknesses. Knowing the pointwise position $\mathbf{x}^{\mathrm{REF}}$, we can find (in parallel) the closest nodal coordinates on the upper and lower AC surfaces using an algorithm of the nearest neighbor searching [5]. In this way,

$$z = \frac{d_t}{d_t + d_b}, \tag{9}$$

where d_t and d_b are respectively the distances to the closest points in the AC top and bottom surfaces.

Furthermore, in 2D models, e.g., [9, 10], the fibrillar orientations have been defined in terms of the coordinate basis vectors of the symmetry plane (containing the primary fibrils). However, since our large-scale model is not symmetrical, we define a local plane at each point, taking into account the fact that the primary fibrils inside this plane in the AC surface form split lines that are roughly directed toward the center of each cartilage substructure [6]. This local plane can then be determined as it contains one vector pointing towards the central point as well as another vector that connects the closest points on the surfaces. Figure 1 provides a visual example of these vectors, illustrated with blue arrows.

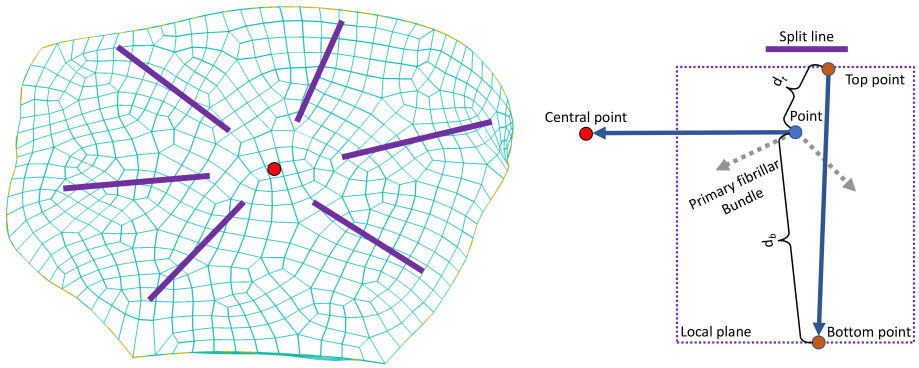

Fig. 1. Example of split line orientations on a cartilage substructure (left) and a local plane of a point (right).

The fibrillar model employed in this study is based on the Wilson et al. model [15], while the non-fibrillar component is a modified neo-Hookean model that accounts for the dependency of solid volume fraction and tissue compressibility [16, 8]. The osmotic pressure is defined using the Poisson–Boltzmann cell model [13, 1]. Readers may refer to these studies for further details.

2.2 Pre-stressing algorithm

The initial values of the parameters affected by the pre-stressing in the numerical model are denoted by $\mathbf{s}$ and include the positional data $\mathbf{x}$ and the constitutive data $\mathbf{m}$ (i.e., components of $\mathbf{n}$, $\emptyset^{\mathrm{S}}$, and ρ^{COL}). The PSA then performs the following stepwise analyses according to

$$\mathbf{s}_0^{(t)} \xrightarrow{\text{forward analysis}} \mathbf{x}_0^{(t+1)} \xrightarrow{\text{backward analysis}} \mathbf{m}_0^{(t+1)}. \tag{10}$$

Therefore, the forward analysis is used to approximate the stress-free geometry, and the change in the constitutive properties at this state is determined through the backward analysis.

Forward analysis. Applying the pre-stress through (6), on the model with the initial state $\mathbf{s}_0^{(t)}$, one obtains the pre-stressed configuration $\hat{\mathbf{x}}^{(t)}$ by an FE analysis and the constitutive model described in the previous subsection. Defining displacement-based update function $\mathbf{u}$ by

$$\mathbf{u}^{(t)} := \hat{\mathbf{x}}^{(t)} - \mathbf{x}^{\mathrm{REF}}, \tag{11}$$

then the stress-free configuration is updated as follows

$$\mathbf{x}_0^{(t+1)} := \begin{cases} \mathbf{x}_0^{(t)} - \zeta^{(t)}\mathbf{u}^{(t)} & \text{if } r^{(\mathrm{t})} \leq r^{(\mathrm{t}-1)}, \\ \mathbf{x}_0^{(t)} & \text{if } r^{(\mathrm{t})} > r^{(\mathrm{t}-1)}, \end{cases} \tag{12}$$

where ζ is a scaling parameter and r is the residual, both determined by the optimizer.

Backward analysis. By confining all AC points with the following displacement-based boundary condition $\mathbf{b}$ (distributed on the FE nodes), i.e.

$$\mathbf{b}^{(t+1)} := \begin{cases} -\zeta^{(t)}\mathbf{u}^{(t)} & \text{if } r^{(\mathrm{t})} \leq r^{(\mathrm{t}-1)}, \\ \mathbf{0} & \text{if } r^{(\mathrm{t})} > r^{(\mathrm{t}-1)}, \end{cases} \tag{13}$$

then an FE analysis can calculate the updated material state $\mathbf{m}_0^{(t+1)}$ via (7) and (8), provided that the analysis starts with state $\mathbf{s}_0^{(t)}$, i.e.

$$\mathbf{n}_0^{(t+1)} = \frac{\check{\mathbf{F}}^{(t)}\mathbf{n}_0^{(t)}}{\left\|\check{\mathbf{F}}^{(t)}\mathbf{n}_0^{(t)}\right\|_2}, \tag{14}$$

$$\forall \varphi \in \left\{\emptyset^{\mathrm{S}},\ \rho^{\mathrm{COL}}\right\}, \qquad \varphi_0^{(t+1)} = \frac{\varphi_0^{(t)}}{\det\check{\mathbf{F}}^{(\mathrm{t})}}. \tag{15}$$

Here, $\check{\mathbf{F}}$ is the deformation gradient of the inverse analysis determined by the solver after applying the nodal condition.

Optimization. Starting with

$$\mathbf{s}_0^{(0)} := \mathbf{s}^{\mathrm{REF}}, \quad \mathbf{u}^{(0)} := \mathbf{0}, \quad \zeta^{(0)} := 1, \quad r^{(0)} := \infty, \quad \mathbf{b}^{(0)} := \mathbf{0}, \quad \check{\mathbf{F}}^{(0)} := \mathbf{I}, \tag{16}$$

then using (10), the updated initial state $\mathbf{s}_0^{(t+1)}$, including both $\mathbf{m}_0^{(t+1)}$ and $\mathbf{x}_0^{(t+1)}$, is obtained. This operation also requires the following definitions

$$\zeta^{(t)} := \begin{cases} \zeta^{(t-1)} & \text{if } r^{(\mathrm{t})} \leq r^{(\mathrm{t}-1)}, \\ \dfrac{\zeta^{(t-1)}}{\eta} & \text{if } r^{(\mathrm{t})} > r^{(\mathrm{t}-1)}, \end{cases} \tag{17}$$

$$r^{(t)} := \left\|\mathbf{U}^{(t)}\right\|_2, \tag{18}$$

where $\mathbf{U}$ is a vector containing all components of $\mathbf{u}$ at all AC nodes, and $\eta = 4$ is a hyperparameter used to avoid possible divergence (and can be varied if convergence is not achievable). It is assumed that the optimization converges as soon as the error calculated from (18) becomes very small, leading to the approximated stress-free state $\mathbf{s}_0$.

2.3 Implementation

The boundary conditions and the FE mesh used are identical to the 3D model used in our previous work [11], but with the second-order elements for higher accuracy, which was developed on the basis of the Open Knee tibiofemoral model

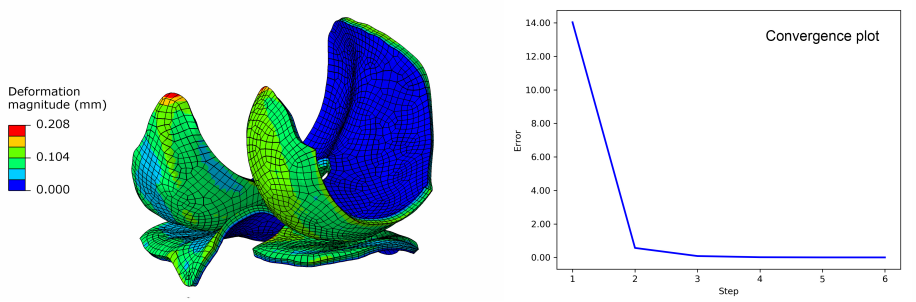

Fig. 2. Contour of cartilage deformation by pre-stress (left) and the convergence diagram of its pre-stressing algorithm (right).

[2]. However, there are two differences: (i) the constitutive model is now multiphasic with the PSA; (ii) no external force is applied to the joint, so we can focus solely on the effect of pre-stressing. Apart from the PSA code updates mentioned above, the implementation of the constitutive model and PSA is similar to our previous study [9]. Interested readers can find further details on the exact implementation steps and the selected values for material parameters in that study.

3 Results and Discussion

In this study, a PSA algorithm with a unified optimizer for AC is presented. This algorithm proved to be sufficiently efficient, taking about six hours (and 6 steps) to fully converge for the tibiofemoral model. Figure 2 (right) illustrates the convergence diagram. In particular, it shows that the running time could be further reduced at the expense of a slight gross error of 0.01. In contrast, our previously implemented PSA [9], which used two separate optimizers, failed to converge even after 12 hours with first-order elements (on a regular computer).

Figure 2 (left) shows the final calculated deformation after the pre-stressing equilibrium, demonstrating that the superficial layer has the highest deformation (up to contact). This is because this zone is not fully constrained or pressurized, and therefore, the pre-stressing might be neglected in damage models that focus on the stress values of the superficial zones. However, the deeper zones do not follow the same pattern.

The deeper layers exhibit the least deformation due to their attachment to the subchondral bones. Figure 3 illustrates the fibrillar von Mises stress in this constrained layer, which is close to the total stress. These values are less than 0.2, comparable to the stresses observed in the literature under 10% strain in compression tests [8, 10], highlighting the significant influence of pre-stressing. Furthermore, these values could be indirectly validated by reference to pre-stresses derived from linear triphasic modeling [3, 12], which vary below 0.4 MPa depend-

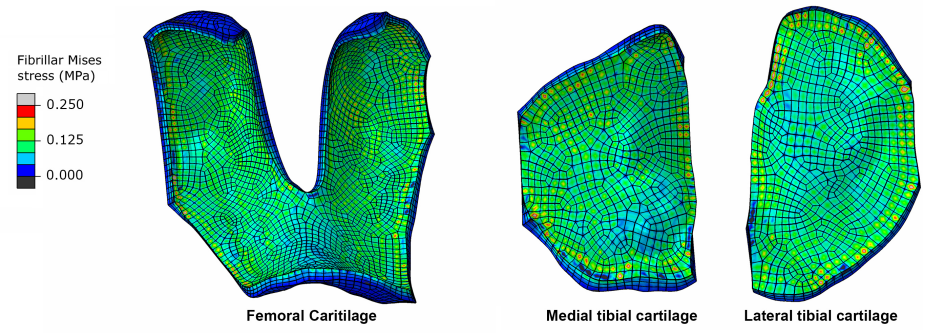

Fig. 3. Recorded stresses of the pre-stressed cartilage substructures. Values in the contacting surfaces are negligible and therefore not shown.

ing on the stress direction. This is within an acceptable range, considering the different geometric and mechanical modeling and calibration.

A potential limitation of this computational model lies in its highly discrete organization of the fibrillar component in the constitutive equation. Consequently, models reliant on fibrillar stress may experience non-physiological stress concentrations. Addressing this issue could involve the use of higher-order elements, a denser or more regular mesh, or the adoption of a less discrete anisotropic equation, possibly through a fibril distribution function [4].

4 Conclusions

To our knowledge, this study is the first to explore pre-stressing in a large-scale AC model, incorporating depth-dependent material properties. The findings reveal that pre-stressing can cause significant deformation, up to approximately 15% of the tissue thickness. This underscores the necessity of accurately identifying the stress-free state. Given the efficiency of the proposed PSA in determining both the stress-free state and pre-stressed conditions, we conclude that this approach is highly applicable in AC research, particularly where the osmotic pressure is a critical factor.

References

1. Buschmann, M. & Grodzinsky, A. A Molecular Model of Proteoglycan-Associated Electrostatic Forces in Cartilage Mechanics. J. Biomech. Eng. 117(5), 179–192 (1995). doi:10.1115/1.2796000
2. Erdemir, A.: Open knee: Open source modeling and simulation in knee biomechanics. J. Knee Surg. 29(2), 107–116 (2016). doi:10.1055/s-0035-1564600
3. Lai, W.M., Hou, J.S., Mow, V.C.: A triphasic theory for the swelling and deformation behaviors of articular cartilage. J. Biomech. Eng. 113(3), 245–258 (1991) doi:10.1115/1.2894880

4. Lei, F. & Szeri, A.Z.: The influence of fibril organization on the mechanical behaviour of articular cartilage. Proc. R. Soc. A: Math. Phys. Eng. 462, 3301–3322 (2006). doi:10.1098/rspa.2006.1732
5. Maneewongvatana, S., Mount, D.: Analysis of approximate nearest neighbor searching with clustered point sets. In: Goldwasser, M.H., Johnson, D.S., McGeoch, C.C. (eds.) Data Structures, Near Neighbor Searches, and Methodology: Fifth and Sixth DIMACS Implementation Challenges, Proceedings of a DIMACS Workshop, USA, 1999, vol. 59, pp. 105–123 (1999). doi:10.48550/arXiv.cs/9901013
6. Mononen, M.E., Mikkola, M.T., Julkunen, P., Ojala, R., Nieminen, M.T., Jurvelin, J.S., Korhonen, R.K.: Effect of superficial collagen patterns and fibrillation of femoral articular cartilage on knee joint mechanics – A 3D finite element analysis. J. Biomech. 45(3), 579–587 (2012), doi:10.1016/j.jbiomech.2011.11.003
7. Mow, V.C., Kuei, S.C., Lai, W.M., Armstrong, C.G.: Biphasic creep and stress relaxation of articular cartilage in compression: Theory and experiments. J. Biomech. Eng. 102(1), 73–84 (1980). doi:10.1115/1.3138202
8. Sajjadinia, S.S., Haghpanahi, M., Razi, M.: Computational simulation of the multiphasic degeneration of the bone-cartilage unit during osteoarthritis via indentation and unconfined compression tests. Proc. Inst. Mech. Eng. H: J. Eng. Med. 233, 871–882 (2019). doi:10.1177/0954411919854011
9. Sajjadinia, S.S., Carpentieri, B., Holzapfel, G.A.: A backward pre-stressing algorithm for efficient finite element implementation of in vivo material and geometrical parameters into fibril-reinforced mixture models of articular cartilage. J. Mech. Behav. Biomed. Mater. 114, 104203 (2021). doi:10.1016/j.jmbbm.2020.104203
10. Sajjadinia, S.S., Haghpanahi, M.: A parametric study on the mechanical role of fibrillar rotations in an articular cartilage finite element model. Sci. Iran. 28(2), 830–836 (2021). doi:10.1007/s10237-006-0044-z
11. Sajjadinia, S.S., Carpentieri, B., Shriram, D., Holzapfel, G.A.: Multi-fidelity surrogate modeling through hybrid machine learning for biomechanical and finite element analysis of soft tissues. Comput. Biol. Med. 148, 105699 (2022). doi:10.1016/j.compbiomed.2022.105699
12. Setton, L.A., Gu, W., Lai, W.M., Mow, V.C.: Predictions of the swelling-induced pre-stress in articular cartilage. In: Selvadurai, A. P. S. (ed.) Mechanics of Poroelastic Media. pp. 299–320, Springer Netherlands (1996). doi:10.1007/978-94-015-8698-6_17
13. Stender, M.E., Raub, C.B., Yamauchi, K.A., Shirazi, R., Vena, P., Sah, R.L., Hazelwood, S.J., Klisch, S.M.: Integrating qPLM and biomechanical test data with an anisotropic fiber distribution model and predictions of TGF-β1 and IGF-1 regulation of articular cartilage fiber modulus. Biomech. Model. Mechanobiol. 12(6), 1073–1088 (2013). doi:10.1007/s10237-012-0463-y
14. Wang, X., Eriksson, T.S.E., Ricken, T., Pierce, D.M.: On incorporating osmotic prestretch/prestress in image-driven finite element simulations of cartilage. J. Mech. Behav. Biomed. Mater. 86, 409–422 (2018). doi:10.1016/j.jmbbm.2018.06.014
15. Wilson, W., van Donkelaar, C.C., van Rietbergen, B., Ito K., Huiskes, R.: Stresses in the local collagen network of articular cartilage: A poroviscoelastic fibril-reinforced finite element study. J. Biomech. 37(3), 357–366 (2004). doi:10.1016/S0021-9290(03)00267-7
16. Wilson, W., Huyghe, J.M., van Donkelaar, C.C.: Depth-dependent compressive equilibrium properties of articular cartilage explained by its composition. Biomech. Model. Mechanobiol. 6(1), 43–53 (2007). doi:10.1007/s10237-006-0044-z